Article

Ion-Enhanced Etching Characteristics of sp^2-Rich Hydrogenated Amorphous Carbons in CF$_4$ Plasmas and O$_2$ Plasmas

Jie Li [1], Yongjae Kim [2], Seunghun Han [1] and Heeyeop Chae [1,2,*]

1   School of Chemical Engineering, Sungkyunkwan University (SKKU), Suwon 16419, Korea;
     lj870408@skku.edu (J.L.); hsh12040@naver.com (S.H.)
2   Sungkyunkwan Advanced Institute of Nanotechnology (SAINT), Sungkyunkwan University (SKKU),
     Suwon 16419, Korea; yon521@skku.edu
*   Correspondence: hchae@skku.edu; Tel.: +82-31-290-7342

Abstract: The sp^2-rich hydrogenated amorphous carbon (a-C:H) is widely adopted as hard masks in semiconductor-device fabrication processes. The ion-enhanced etch characteristics of sp^2-rich a-C:H films on ion density and ion energy were investigated in CF$_4$ plasmas and O$_2$ plasmas in this work. The etch rate of sp^2-rich a-C:H films in O$_2$ plasmas increased linearly with ion density when no bias power was applied, while the fluorocarbon deposition was observed in CF$_4$ plasmas instead of etching without bias power. The etch rate was found to be dependent on the half-order curve of ion energy in both CF$_4$ plasmas and O$_2$ plasmas when bias power was applied. An ion-enhanced etching model was suggested to fit the etch rates of a-C:H in CF$_4$ plasmas and O$_2$ plasmas. Then, the etch yield and the threshold energy for etching were determined based on this model from experimental etch rates in CF$_4$ plasma and O$_2$ plasma. The etch yield of 3.45 was observed in CF$_4$ plasmas, while 12.3 was obtained in O$_2$ plasmas, owing to the high reactivity of O radicals with carbon atoms. The threshold energy of 12 eV for a-C:H etching was obtained in O$_2$ plasmas, while the high threshold energy of 156 eV was observed in CF$_4$ plasmas. This high threshold energy is attributed to the formation of a fluorocarbon layer that protects the a-C:H films from ion-enhanced etching.

Keywords: sp^2-rich hydrogenated amorphous carbon; ion-enhanced etching; CF$_4$ and O$_2$ plasma etching

1. Introduction

Recently, carbons at the nanoscale attract great interest for a huge number of applications, such as transistor, field emission display, actuator, molecular wires/interconnect, transparent conducting film, supercapacitor, and catalyst [1–8]. Especially hydrogenated amorphous carbon (a-C:H) layers are widely used as a hard mask in semiconductor-device fabrication processes. The a-C:H layers are replacing conventional organic photoresists in high-aspect-ratio etching processes because they can provide a higher etch resistance and etch selectivity than photoresists to various harsh etching chemicals, such as fluorocarbon plasmas [9–11]. Moreover, a-C:H films are also attractive because they are easy to be removed with oxygen plasmas when they are compared with other non-carbon inorganic mask materials. The a-C:H hard mask contains sp^2 carbons and sp^3 carbons, and its sp^2/sp^3 ratio is strongly related to the physical and chemical properties of a-C:H hard mask films [12–17]. In general, higher film density, stronger film hardness, and higher etching resistance are observed in higher sp^2/sp^3 ratio of a-C:H films. Therefore, a-C:H films with high sp^2/sp^3 ratio, or sp^2-rich a-C:H films are preferred over sp^3-rich a-C:H for hard mask applications in semiconductor processes [9,18].

The understanding of etching characteristics and mechanism of sp^2-rich a-C:H hard mask in plasmas is required for highly selective high-aspect-ratio etching processes, and the etching characteristics have been studied by several research groups [19–22]. The etching of sp^2-rich a-C:H can be characterized by the etch yield and the threshold energy. The etch yield is defined as the number of carbon atoms removed by each incident ion and is affected

by the reactivity of ions, ion energy, and surface composition. The threshold energy is the minimum energy of ion required for carbon removal and is affected by the reactivity of etched films. A relatively low etch yield of 0.26 at ion energy of 400 eV was reported for sp^2-rich a-C:H by physical sputtering in non-reactive Ar plasmas [19]. A lot higher etch yield of 4.3 was reported for sp^2-rich a-C:H films when the carbon films were exposed to Ar^+ ions and O_2, indicating the O_2 molecules enhance etch reaction of carbons significantly [20]. Hansen et al. determined the threshold energy of a-C:H for etching in a cascaded arc Ar/H_2 plasma and they reported the significant decrease of threshold energy to 3–5 eV with H radicals from 58 eV without H radicals [21]. Salonen et al. reported a high etch yield of 1.0 and a low threshold energy of 1.0 eV in a mixture of H^+ ions and H atoms, using classical molecular-dynamics simulations [22]. Fluorocarbon plasmas are typically adopted for patterning processes with a-C:H hard masks, and O_2 plasmas are applied for the removal of residual a-C:H hard masks in many dielectric etch processes, but few research studies on a-C:H etching have been reported in theses plasmas [23,24]. In addition, the direct effect of ions on a-C:H etching in fluorocarbon and O_2 plasmas is hardly studied.

In this work, the effect of ions on the sp^2-rich a-C:H etch was investigated in CF_4 plasmas and O_2 plasmas by measuring etch rates at different ion density and ion energy. An ion-enhanced etching model was suggested to fit the etch mechanism of sp^2-rich a-C:H films in CF_4 plasmas and O_2 plasmas. The etch yield and threshold energy were determined from experimental etch rates fitted on this model, and the etch yield and threshold energy were compared with those reported in previous researches in various conditions. The chemical compositions of a-C:H films after etching in CF_4 and O_2 plasmas were also investigated.

2. Experimental Setup and Procedures

The a-C:H films used in this work were deposited in a C_2H_2 plasma in an inductively coupled plasma (ICP) reactor with 250 W power and 21 mTorr process pressure. The a-C:H films of about 600 nm were obtained after deposition of 15 min and were determined by ellipsometry. The a-C:H films were characterized by X-ray photoelectron spectroscopy (XPS), where the C 1s peak was deconvoluted into three peaks of the sp^2 (284.5 eV), sp^3 (285.2 eV), and CO band (286.5 eV) by Gaussian fitting, as shown in Figure 1a. The sp^2/sp^3 ratio of a-C:H films was 1.70 determined by the relative intensity of the sp^2 versus sp^3 peak, and is similar with the number reported in a previous research [9]. The a-C:H films were also characterized by Raman spectroscopy and the Raman spectrum was deconvoluted into D and G peaks by Gaussian fitting, as shown in Figure 1b. The intensity ratios of the D and G peaks (I_D/I_G) in the Raman spectrum can indicate the sp^2/sp^3 ratio, because the D peak contains information on sp^2 carbons only, while the G peak provides information on both sp^2 and sp^3 carbons [25,26]. An I_D/I_G of 2.0 was obtained in a-C:H films; that is similar to the I_D/I_G reported in previous researches [26].

The sp^2-rich a-C:H films were etched in CF_4 and O_2 plasmas in another ICP chamber, as shown in Figure 1c. This ICP reactor was operated with a source power of 13.56 MHz radio frequency (RF) and a bias power of 12.56 MHz. The source power was delivered through an inductive coil on the top of a quartz window and the bias power was delivered through a bottom electrode. The a-C:H films were placed on the center of a 100 mm silicon wafer and on the top of a ceramic electrostatic chuck, which was positioned on the bottom electrode. The reactor was evacuated to 5 mTorr before introducing the etching gas, and after introducing 20 sccm CF_4 or O_2, the reactor pressure was maintained at 100 mTorr. CF_4 plasmas and O_2 plasmas were generated with the source power of 50~250 W and bias power of 0~50 W, and sp^2-rich a-C:H films were etched in these plasmas for 1 min. The chemical compositions of sp^2-rich a-C:H films were investigated after 1 min CF_4 and O_2 plasma etching with 250 W source power and 10 W bias power.

(a)

(b)

(c)
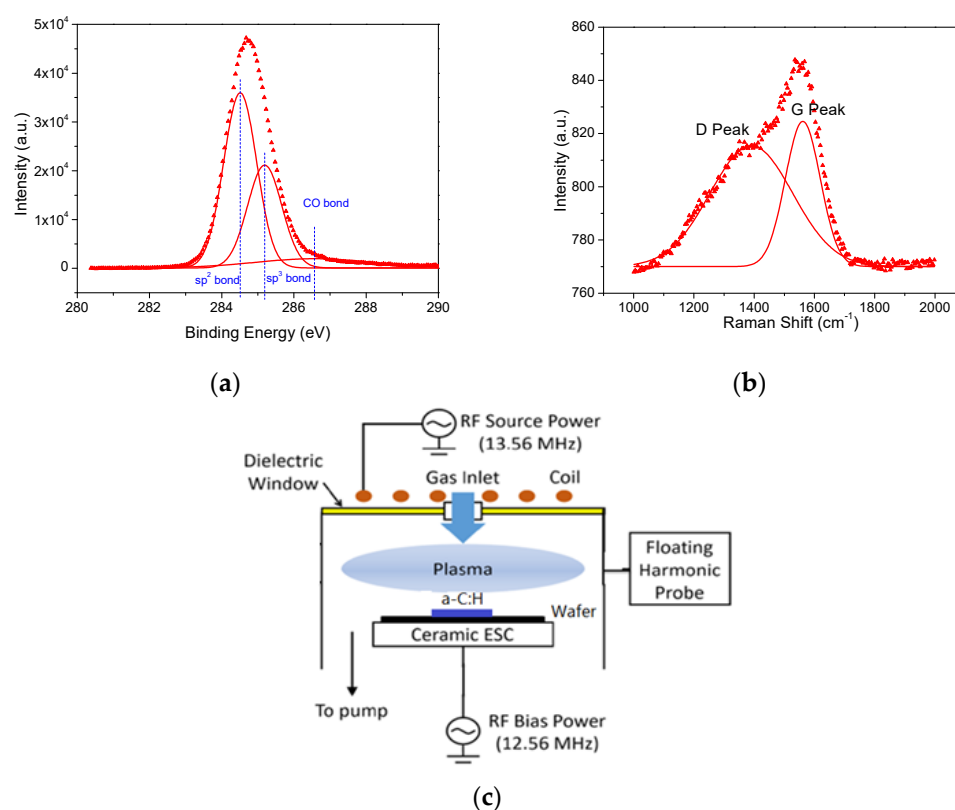
Figure 1. (**a**) XPS C1s profile of a-C:H films deposited in the C_2H_2 ICP plasma. C1s spectrum of a-C:H was deconvoluted into three bands (sp^2 bands, sp^3 bands, and CO bands) by Gaussian fitting. (**b**) Raman spectrum of a-C:H films. Raman spectrum of a-C:H was deconvoluted into D and G peaks by Gaussian fitting. (**c**) Schematic diagram of ICP chamber used in this work.

The ion density in plasmas was measured by using a floating harmonic probe (WiseProbe, P&A solutions, Seoul, Korea), and the bias voltage was determined by a VI probe (Octiv Poly, Impedans, Dublin, Ireland). The etch rates of a-C:H films were determined by measuring the thickness of the a-C:H films with an ellipsometer (SE MF-1000, NanoView, Ansan, Korea) before and after etching processes. The chemical compositions of a-C:H films before and after etching processes were analyzed with XPS (Escalab 250, Thermo-Scientific, Waltham, MA, USA).

3. Results and Discussion

Ion density and ion energy were determined for the plasmas generated with the varied source power and bias power, and these values are plotted in Figure 2 as a first step. The ion density is 2.5–3.0 times higher in O_2 plasmas than in CF_4 plasmas, as shown in Figure 2a,b, and this is attributed to the low ionization energy of oxygen atoms (13.6 eV) compared with that of fluorine atoms (17.4 eV). The ion density increases by 3.9 and 3.7 times in CF_4 and O_2 plasmas in the source power range of 50~250 W, respectively. The ion density increases about 60% in both CF_4 and O_2 plasmas with bias power in the range of 0~50 W, indicating that ion density is affected more significantly by the source power than bias power. The ion energy in plasmas was estimated from the bias voltage as shown in Figure 2c. The effect of source power on ion energy is marginal in ICP plasmas [27], and the ion energy increases by 2.1 times in both CF_4 and O_2 plasmas with increased bias power from 10 to 50 W. The ion energy in CF_4 plasmas is slightly higher than that in O_2 plasmas probably due to the higher sheath potential resulting from the lower ion density in CF_4 plasmas.
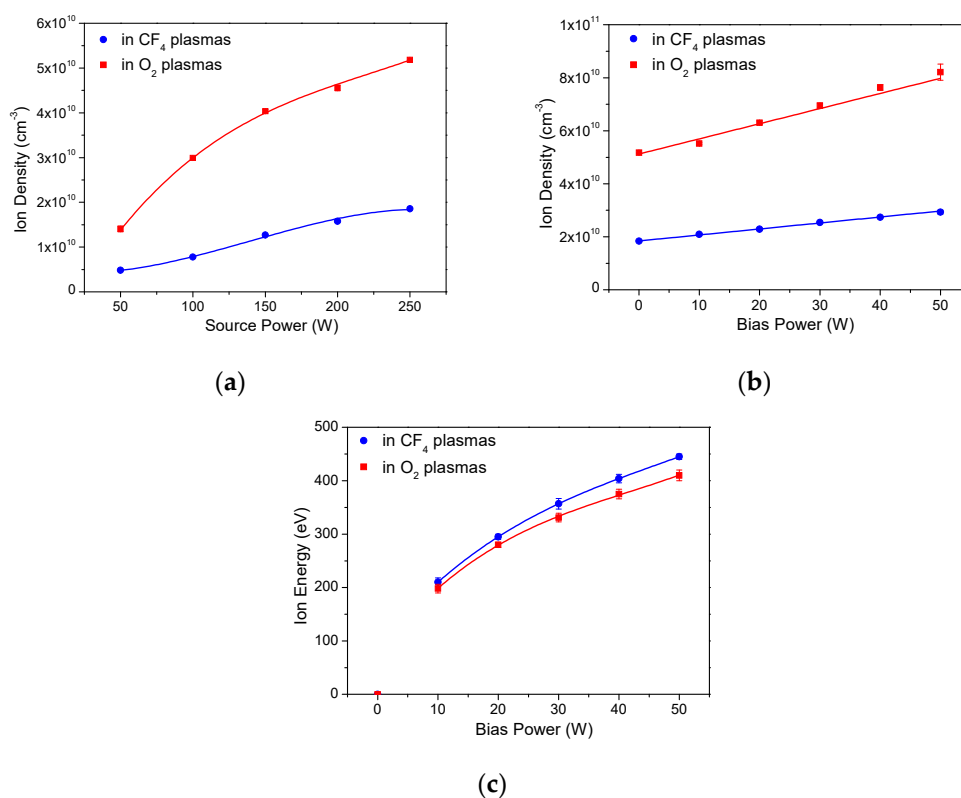
Figure 2. (**a**) Ion density in CF_4 plasmas and O_2 plasmas without bias power as a function of source power. (**b**) Ion density in CF_4 plasmas and O_2 plasmas with 250 W source power as a function of bias power. (**c**) Ion energy in CF_4 plasmas and O_2 plasmas with 250 W source power as a function of bias power.

The etch-rate dependences of sp^2-rich a-C:H on source power and bias power were investigated in CF_4 plasmas and O_2 plasmas shown in Figure 3 as the next step. The etch rate of a-C:H in O_2 plasmas increases from 2.3 to 7.0 nm/min with increased source power even without bias power as shown in Figure 3a. This is attributed to the increased density of O radicals in O_2 plasmas with the increased source power. The O radicals are expected to be chemisorbed on the surface of a-C:H films with the low activation energy of 0.046 eV and react with carbons for carbon removal with the activation energy of 0.28 eV by oxidization in O_2 plasmas [28,29]. In CF_4 plasmas, slight film deposition was observed on the surface of a-C:H films instead of etching when no bias power was applied. The fluorocarbon deposition was also reported on the outer and inner surface of carbon nanotube in CF_4 plasmas [30]. The F radicals are easily chemisorbed on carbon surface with a low activation energy of 0.13 eV, but it was reported that it is difficult to remove the carbons due to the high activation energy of 0.56–2.4 eV for removal reactions [31]. The etch rate of a-C:H was measured with bias power, as shown in Figure 3b. The etch rate increases from 0 to 51 nm/min when the bias power increases from 0 to 50 W in CF_4 plasmas. Ions are accelerated and bombarded with the bias power, and the ions break C-C and C-H bonds and create dangling bonds on the surface of films, which allows the carbon removal with F radicals with low activation energy. A sharp increase of etch rate of sp^2-rich a-C:H from 7.0 to 510 nm/min was observed with increased bias power in the range of 0~50 W in O_2 plasmas, indicating the etching is accelerated with the energetic ions.

The etch rate of sp^2-rich a-C:H was correlated with ion density and ion energy separately to investigate the etching mechanism in CF_4 plasmas and O_2 plasmas, as shown in Figure 4. The etch rate of sp^2-rich a-C:H increases linearly with ion density in O_2 plasmas, as shown in Figure 4a. The creation of dangling bonds by bombarding ions accelerates the carbon reaction with O radicals [23]. The etch rate is affected by ion energy and ion density

obviously, and it was normalized to exclude the effect of ion density by dividing the etch rate with the ratio of ion density with and without bias power, as shown in Equation (1):

$$ER_{normalized} = ER_{orginal} * \frac{n_i(\text{without bias power})}{n_i(\text{with bias power})} \tag{1}$$

where ER is the etch rate, and n_i is the ion density in plasmas. The effect of ion energy on the etch rate of sp^2-rich a-C:H films is plotted in Figure 4b. The normalized etch rate of sp^2-rich a-C:H fits well with half-order curves of ion energy in CF_4 plasmas and O_2 plasmas. The ions of high energy help in breaking C–C and C–H bonds and creating dangling bonds on the surface of films in each bombarding, and active radicals react with these dangling bonds, resulting in the etching of carbon atoms [32]. This significant enhancement of etch rate with bias power indicates that the creation of dangling bonds by energetic ions is believed to be limiting factor in the carbon removal.

(**a**)   (**b**)
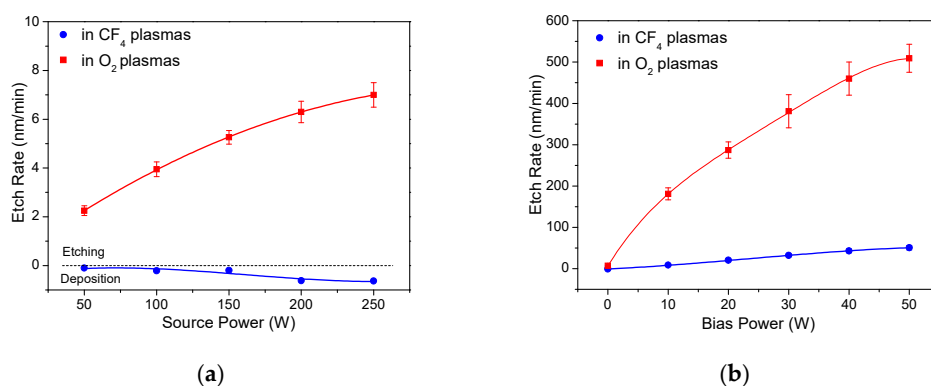
Figure 3. (**a**) Etch rates of sp^2-rich a-C:H in plasmas without bias power as a function of source power. (**b**) Etch rates of sp^2-rich a-C:H in plasmas with 250 W source power as a function of bias power.

(**a**)   (**b**)
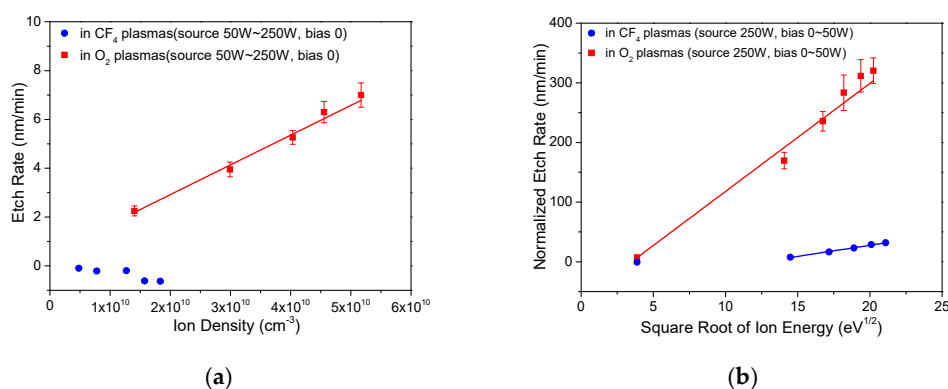
Figure 4. (**a**) Etch rates of sp^2-rich a-C:H as a function of ion density. (**b**) Normalized etch rates of sp^2-rich a-C:H as a function of square root of ion energy.

A model of ion-enhanced etching was developed with the following equations and plotted in Figure 5 [33].

$$R = YI/\rho \tag{2}$$

where R is the etch rate, Y is the etch yield, I is the ion flux, and ρ is the density of a-C:H (1.9 g/cm³) [9]. The etch yield of sp^2-rich a-C:H calculated by Equation (2) increases linearly with the square root of ion energy in CF_4 plasmas and O_2 plasmas, as shown in Figure 5a.

The etch yield of 3.45 and 12.3 was obtained in CF_4 and O_2 plasmas, respectively, at 400 eV. The etch yield, Y, can be described by Equation (3) [34]:

$$Y = b\left(E^{\frac{1}{2}} - E_{th}^{\frac{1}{2}}\right) \tag{3}$$

where b is the proportional parameter, E is the ion energy, and E_{th} is the threshold energy. The coefficients b and E_{th} in Equation (3) were determined as the slope and the horizontal intercept in the etch yield and ion energy plot, as shown in Figure 5a and Table 1. The etch rates of sp^2-rich a-C:H were modeled with these b and E_{th}, and this model agrees well with experimental etch rates, as shown in Figure 5b, indicating that the ion-enhanced etching fits the etching mechanism of sp^2-rich a-C:H in CF_4 plasmas and O_2 plasmas well.


(a)	**(b)**
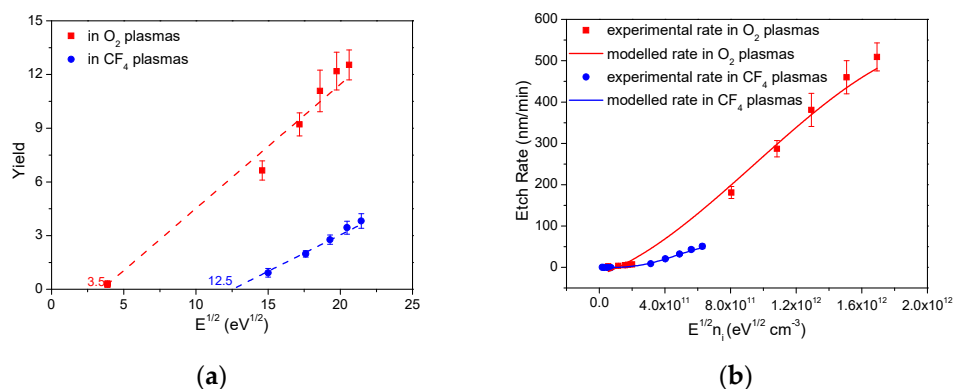
Figure 5. (**a**) Etch yield of sp^2-rich a-C:H as a function of $E^{1/2}$ in CF_4 plasmas and O_2 plasmas. E is the ion energy. (**b**) Etch rates of sp^2-rich a-C:H as a function of $E^{1/2}n_i$ in CF_4 plasmas and O_2 plasmas. n_i is the ion density. Experimental data and modeling data are listed for comparison.

Table 1. Coefficients in ion-enhanced etch modeling used in this work.

| a-C:H	$b(eV^{-1/2})$	$E_{th}(eV)$
in CF_4 plasmas	0.4	156
in O_2 plasmas	0.65	12

The etch yield and the threshold energy obtained in CF_4 plasmas and O_2 plasmas were compared with those reported values in previous works of carbon etching with Ar^+ ions only, Ar^+ ions/O_2 molecules and Ar^+ ions/H radicals [19–22,32,35–38]. The etch yield at 400 eV is plotted in Figure 6a from the results of these researches. The highest etch yield (12.3) was observed in O_2 plasmas among these systems, due to the extremely high activity of O radicals with carbon atoms. The activation energy of carbon removal is as low as 0.28 eV in O_2 plasmas, as mentioned earlier [29]. The etch yield in CF_4 plasmas (3.45) is lower than that in Ar^+ ions/O_2 molecules (4.25), but higher than that in Ar^+ ions/H radicals (2), indicating the reactivity of F radicals with carbons is lower than O_2 molecules and higher than H radicals. This is also proven with the activation energy of carbon removal in CF_4 plasma (0.56–2.4 eV), which is higher than that of carbon reaction with O_2 molecules (0.46 eV) and lower than that of carbon removal with H radicals (1.6–2.5 eV) [21,38]. The relatively low etch yield was also found in carbon etching with inert Xe^+, Ar^+, and N_2^+ without any radical/reactive molecules on surface. The threshold energy measurements of a-C:H in CF_4 plasmas and O_2 plasmas are notated with those in different environments, in Figure 6b. The quite high threshold energy of 156 eV was observed in CF_4 plasmas, and it is attributed to the formation of fluorocarbon layer on the surface of sp^2-rich a-C:H films. This fluorocarbon layer is expected to protect a-C:H films from ion-enhanced etching by protecting C-C bonds. The threshold energies reported in H^+

ions/H radicals (1 eV), Ar^+ ions/H radicals (1.3 eV), and H_2 plasmas (3 eV) are lower than that in O_2 plasmas (12 eV) of this work. H radicals are smaller than O radicals, making them more easily penetrate into sp^2-rich a-C:H films. These H radicals in a-C:H films are believed to transfer sp^2-carbons into sp^3-carbons by forming C-H bonds and decrease the bonding energy in a-C:H films, resulting in the decrease of etch threshold energy.

(a)

(b)
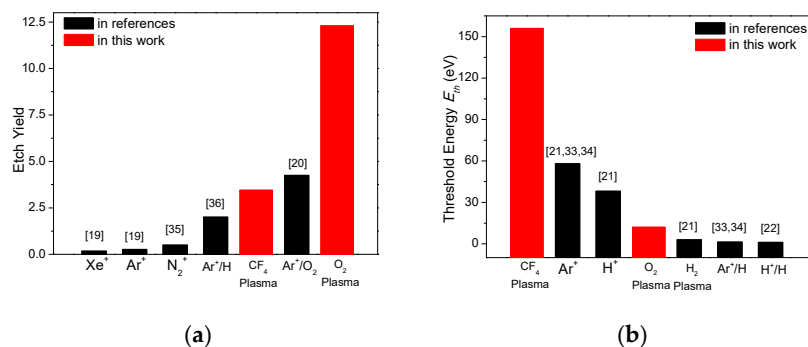
Figure 6. (**a**) The etch yield in CF_4 plasmas and O_2 plasmas in this work and other systems reported in references. The yield was collected with electron energy of 400 eV. (**b**) The threshold energy in CF_4 plasmas and O_2 plasmas in this work and other systems reported in references.

Chemical compositions of a-C:H films were investigated after CF_4 plasmas and O_2 plasmas etching with XPS analysis, as shown in Figure 7a. The chemical compositions of a-C:H films were determined from the peak areas and are presented in Figure 7b. In total, 29% of fluorine was found to be included in a-C:H films after CF_4 plasma etching; that is higher than oxygen atomic percentage of 15% in a-C:H films after O_2 plasma etching. The fluorocarbon layers on the surface of carbon films are expected to form in CF_4 plasmas, but residual oxygen atoms are more difficult to stay in carbon films after O_2 plasma etching. Similar phenomena were reported in the carbon nanotube exposed to CF_4 plasma and O_2 plasma [30]. The CF, CF_2, and CF_3 bonds are observed in XPS C1s spectra after CF_4 plasmas etching, as shown in Figure 7c, indicating the formation of fluorocarbon layer.

(a)

(b)

(c)
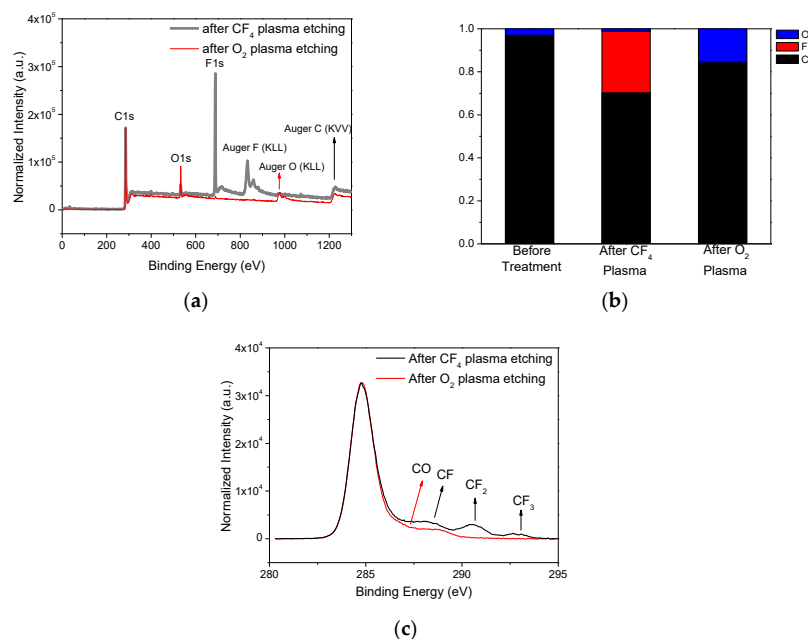
Figure 7. (**a**) XPS of a-C:H after CF_4 and O_2 plasmas etching, (**b**) chemical compositions of a-C:H before and after plasmas etching, and (**c**) XPS C1s profiles of a-C:H after CF_4 and O_2 plasmas etching.

4. Conclusions

Etch characteristics of sp^2-rich a-C:H films were investigated with different ion density and ion energy in CF_4 plasmas and O_2 plasmas. The etch rate of sp^2-rich a-C:H films increases linearly with ion density in O_2 plasmas, while no etch was observed in CF_4 plasmas when no bias power was applied. The a-C:H etch rates in CF_4 plasmas and O_2 plasmas fit well with the half-order curve of ion energy with bias power applied. An ion-enhanced etching model was suggested to fit the etch rates, and the etch yield and threshold energy were estimated from this model. The etch yields of 3.45 in CF_4 plasmas and 12.3 in O_2 plasmas were obtained. The high etch yield in O_2 plasmas is attributed to the high reactivity of O radicals with carbon atoms. The etch threshold energy values of 156 eV in CF_4 plasmas and 12 eV in O_2 plasmas were observed. The high threshold energy in CF_4 plasmas is attributed to the formation of fluorocarbon layers on the surface of sp^2-rich a-C:H films that protects the films from ion-enhanced etching.

References

1. Lin, Y.-M.; Valdes-Garcia, A.; Han, S.-J.; Farmer, D.B.; Meric, I.; Sun, Y.; Wu, Y.; Dimitrakopoulos, C.; Grill, A.; Avouris, P.; et al. Wafer-scale graphene integrated circuit. *Science* **2011**, *332*, 1294–1297. [CrossRef]
2. Wu, Z.-S.; Pei, S.; Ren, W.; Tang, D.; Gao, L.; Liu, B.; Li, F.; Liu, C.; Cheng, H.-M. Field emission of single-layer graphene films prepared by electrophoretic deposition. *Adv. Mater.* **2009**, *21*, 1756–1760. [CrossRef]
3. Aliev, A.E.; Oh, J.; Kozlov, M.E.; Kuznetsov, A.A.; Fang, S.; Fonseca, A.F.; Ovalle, R.; Lima, M.D.; Haque, M.H.; Gartstein, Y.N.; et al. Giant-Stroke, Superelastic Carbon nanotube aerogel muscles. *Science* **2009**, *323*, 1575–1578. [CrossRef]
4. Rueckes, T.; Kim, K.; Joselevich, E.; Tseng, G.Y.; Cheung, C.-L.; Lieber, C.M. Carbon nanotube–based nonvolatile random access memory for molecular computing. *Science* **2000**, *289*, 94–97. [CrossRef] [PubMed]
5. Wang, X.; Zhi, L.; Müllen, K. Transparent, Conductive graphene electrodes for dye-sensitized solar cells. *Nano Lett.* **2008**, *8*, 323–327. [CrossRef]
6. Simon, P.; Gogotsi, Y. Materials for electrochemical capacitors. *Nat. Mater.* **2008**, *7*, 845–854. [CrossRef] [PubMed]
7. Lin, Y.; Sun, X.; Su, D.S.; Centi, G.; Perathoner, S. Catalysis by hybrid sp2/sp3nanodiamonds and their role in the design of advanced nanocarbon materials. *Chem. Soc. Rev.* **2018**, *47*, 8438–8473. [CrossRef]
8. Akay, G. Plasma generating—Chemical looping catalyst synthesis by microwave plasma shock for nitrogen fixation from air and hydrogen production from water for agriculture and energy technologies in global warming prevention. *Catalysts* **2020**, *10*, 152. [CrossRef]
9. Robertson, J. Diamond-like amorphous carbon. *Mater. Sci. Eng. R Rep.* **2002**, *37*, 129–281. [CrossRef]
10. Kwon, B.S.; Kim, J.S.; Lee, N.-E.; Shon, J.W. Ultrahigh Selective Etching of SiO_2 Using an Amorphous Carbon Mask in Dual-Frequency Capacitively Coupled $C_4F_8/CH_2F_2 / O_2/Ar$ Plasmas. *J. Electrochem. Soc.* **2010**, *157*, D135–D141. [CrossRef]
11. Jeon, M.H.; Park, J.W.; Yun, D.H.; Kim, K.N.; Yeom, G.Y. Etch properties of amorphous carbon material using RF pulsing in the $O_2/N_2/CHF_3$ plasma. *J. Nanosci. Nanotechnol.* **2015**, *15*, 8577–8583. [CrossRef]
12. Robertson, J. Amorphous carbon. *Adv. Phys.* **1986**, *35*, 317–374. [CrossRef]
13. Robertson, J.; O'Reilly, E.P. Electronic and atomic structure of amorphous carbon. *Phys. Rev. B* **1987**, *35*, 2946–2957. [CrossRef]

14. Robertson, J. Hard amorphous (diamond-like) carbons. *Prog. Solid State Chem.* **1991**, *21*, 199–333. [CrossRef]
15. Akkerman, Z.L.; Efstathiadis, H.; Smith, F.W. Thermal stability of diamondlike carbon films. *J. Appl. Phys.* **1996**, *80*, 3068–3075. [CrossRef]
16. Wang, C.Z.; Ho, K.M. Structure, dynamics, and electronic properties of diamondlike amorphous carbon. *Phys. Rev. Lett.* **1993**, *71*, 1184–1187. [CrossRef]
17. Maitre, N.; Girardeau, T.; Camelio, S.; Barranco, A.; Vouagner, D.; Breelle, E. Effects of negative low self-bias on hydrogenated amorphous carbon films deposited by PECVD technique. *Diam. Relat. Mater.* **2003**, *12*, 988–992. [CrossRef]
18. Hong, J.; Turban, G. Etching process of hydrogenated amorphous carbon (a-C:H) thin films in a dual ECR-r.f. nitrogen plasma. *Diam. Relat. Mater.* **1999**, *8*, 572–576. [CrossRef]
19. Kolasinski, R.D.; Polk, J.E.; Goebel, D.; Johnson, L.K. Carbon sputtering yield measurements at grazing incidence. *Appl. Surf. Sci.* **2008**, *254*, 2506–2515. [CrossRef]
20. Hopf, C.; Schlüter, M.; Jacob, W. Chemical sputtering of carbon films by argon ions and molecular oxygen at cryogenic temperatures. *Appl. Phys. Lett.* **2007**, *90*, 224106. [CrossRef]
21. Hansen, T.T.; Weber, J.J.-W.; Colsters, P.G.J.; Mestrom, D.M.H.G.; Van De Sanden, M.R.; Engeln, R.R. Synergistic etch rates during low-energetic plasma etching of hydrogenated amorphous carbon. *J. Appl. Phys.* **2012**, *112*, 013302. [CrossRef]
22. Salonen, E.; Nordlund, K.; Keinonen, J.; Wu, C.H. Swift chemical sputtering of amorphous hydrogenated carbon. *Phys. Rev. B* **2001**, *63*, 195415. [CrossRef]
23. Ralchenko, V.G.; Kononenko, T.V.; Foursova, T.; Loubnin, E.N. Comparison of laser and O_2 plasma etching of diamond-like carbon films. *Diam. Relat. Mater.* **1993**, *2*, 211–217. [CrossRef]
24. Balachova, O.; Alves, M.; Swart, J.; Braga, E.; Cescato, L. CF_4 plasma etching of materials used in microelectronics manufacturing. *Microelectron. J.* **2000**, *31*, 213–215. [CrossRef]
25. Andújar, J.; Vives, M.; Corbella, C.; Bertran, E. Growth of hydrogenated amorphous carbon films in pulsed d.c. methane discharges. *Diam. Relat. Mater.* **2003**, *12*, 98–104. [CrossRef]
26. Tai, F.C.; Lee, S.C.; Wei, C.H.; Tyan, S.L. Correlation between ID/IG ratio from visible raman spectra and sp2/sp3 ratio from XPS spectra of annealed hydrogenated DLC film. *Mater. Trans.* **2006**, *47*, 1847–1852. [CrossRef]
27. Sobolewski, M.A.; Olthoff, J.K.; Wang, Y. Ion energy distributions and sheath voltages in a radio-frequency-biased, inductively coupled, high-density plasma reactor. *J. Appl. Phys.* **1999**, *85*, 3966–3975. [CrossRef]
28. Teng, H.; Hsieh, C.-T. Activation energy for oxygen chemisorption on carbon at low temperatures. *Ind. Eng. Chem. Res.* **1999**, *38*, 292–297. [CrossRef]
29. Holland, L.; Ojha, S. The chemical sputtering of graphite in an oxygen plasma. *Vacuum* **1976**, *26*, 53–60. [CrossRef]
30. Felten, A.; Bittencourt, C.; Pireaux, J.J.; Van Lier, G.; Charlier, J.C. Radio-frequency plasma functionalization of carbon nanotubes surface O_2, NH_3, and CF_4 treatments. *J. Appl. Phys.* **2005**, *98*, 74308. [CrossRef]
31. Lvova, N.; Ananina, O.; Ryazanova, A. Fluorine and carbon fluoride interaction with a diamond surface: Quantum-chemical modeling. *Comput. Mater. Sci.* **2016**, *124*, 30–36. [CrossRef]
32. Jacob, W.; Hopf, C.; Schlüter, M. Chemical sputtering of carbon materials due to combined bombardment by ions and atomic hydrogen. *Phys. Scr.* **2006**, *T124*, 32–36. [CrossRef]
33. Chae, H.; Sawin, H.H. Plasma kinetic study of silicon-dioxide removal with fluorocompounds in a plasma-enhanced chemical vapor deposition chamber. *J. Korean Phys. Soc.* **2007**, *51*, 978–983. [CrossRef]
34. Steinbruchel, C. Universal energy dependence of physical and ion-enhanced chemical etch yields at low ion energy. *Appl. Phys. Lett.* **1989**, *55*, 1960–1962. [CrossRef]
35. Hopf, C.; Von Keudell, A.; Jacob, W. Chemical sputtering of hydrocarbon films. *J. Appl. Phys.* **2003**, *94*, 2373. [CrossRef]
36. Hopf, C.; Von Keudell, A.; Jacob, W. Chemical sputtering of hydrocarbon films by low-energy Ar ion and H atom impact. *Nucl. Fusion* **2002**, *42*, L27–L30. [CrossRef]
37. Hammer, P.; Gissler, W. Chemical sputtering of carbon films by low energy N_2^+ ion bombardment. *Diam. Relat. Mater.* **1996**, *5*, 1152–1158. [CrossRef]
38. Froberg, R.W.; Essenhigh, R. Reaction order and activation energy of carbon oxidation during internal burning. *Symp. (Int.) Combust.* **1979**, *17*, 179–187. [CrossRef]